A Midlatitude Influence on Australian Monsoon Bursts

SUGATA NARSEY, MICHAEL J. REEDER, DUNCAN ACKERLEY, AND CHRISTIAN JAKOB

School of Earth, Atmosphere and Environment, and Australian Research Council Centre of Excellence for Climate Systems Science, Monash University, Clayton, Victoria, Australia

(Manuscript received 20 September 2016, in final form 27 March 2017)

ABSTRACT

The initiation of northern Australian monsoon rainfall bursts is accompanied by an increase in cyclonic circulation in the monsoon region. This study shows that the change in circulation at the start of the composite rainfall burst is predominantly influenced by midlatitude frontlike features. By exploiting the relationship between circulation tendency and the convergence of absolute vorticity flux, the circulation changes accompanying the initiation of Australian monsoon bursts is investigated. Moisture flux convergence is found to be proportional to the circulation changes in the monsoon region. Using a composite analysis it is shown that absolute vorticity fluxes through the southern boundary are by far the most important influence on monsoon burst circulation changes, with only one-third of events more closely related to other influences including the Madden–Julian oscillation. This is shown to be true throughout the wet season.

1. Introduction

The Australian summer monsoon is the Southern Hemisphere branch of the Asian–Australian monsoon system (Wang 2006). It is an important feature of the tropical Australian climate, delivering a large portion of the northern Australian annual rainfall (Nicholls et al. 1982). The Australian monsoon occurs as a series of active periods characterized by sudden bursts of rainfall, followed by inactive break periods (Drosdowsky 1996; Pope et al. 2009). The present study aims to describe how the circulation changes during the rapid transition from break to burst periods.

We define the Australian monsoon region as the land area 10°–20°S, 120°–150°E (marked inset in Fig. 1). The north Australian wet season occurs between October and April of the following year, and the present study focuses on rainfall in those months. Rainfall averaged over the monsoon region for two example wet seasons is shown in Fig. 1. Sudden bursts of rainfall can be seen followed by periods with low rainfall. Drosdowsky (1996) showed that considerable variability of rainfall bursts and breaks exists in any given season with no preferred length for these periods. It should be noted that bursts are defined in this study using area-averaged rainfall following the method of Berry and Reeder (2016), whereas Drosdowsky (1996) used wind and rainfall observations at Darwin only. Unlike previous studies of Australian monsoon bursts (e.g., Troup 1961), we do not include criteria for rainfall accumulation since the focus of this study is the dynamical influence on sharp transitions from low to high rainfall throughout the wet season.

Extratropical weather systems have been identified previously as one of the factors determining intraseasonal monsoon transitions (e.g., Davidson et al. 1983, 2007). Using a front detection algorithm (Berry et al. 2011), Berry and Reeder (2016) found that the onset of an Australian monsoon burst frequently coincided with the passage of a front across the continent (see their Fig. 5). These frontlike features were associated with midlatitude Rossby waves. Other studies have emphasized the influence of the Madden–Julian oscillation (MJO) on the intraseasonal variability of the Australian monsoon (e.g., Hendon and Liebmann 1990a). Although Berry and Reeder (2016) showed that the MJO was only weakly related to the onset of our defined bursts, they did not address the influence of the MJO on the amount of burst precipitation.

There is a relationship between net circulation and absolute vorticity flux. In order for the vertical vorticity, and therefore the net circulation, in a fixed region to increase, there must be a convergence of absolute vorticity flux through its boundaries (Haynes and McIntyre 1987).

Corresponding author: Sugata Narsey, sugata.narsey@monash.edu

DOI: 10.1175/JCLI-D-16-0686.1

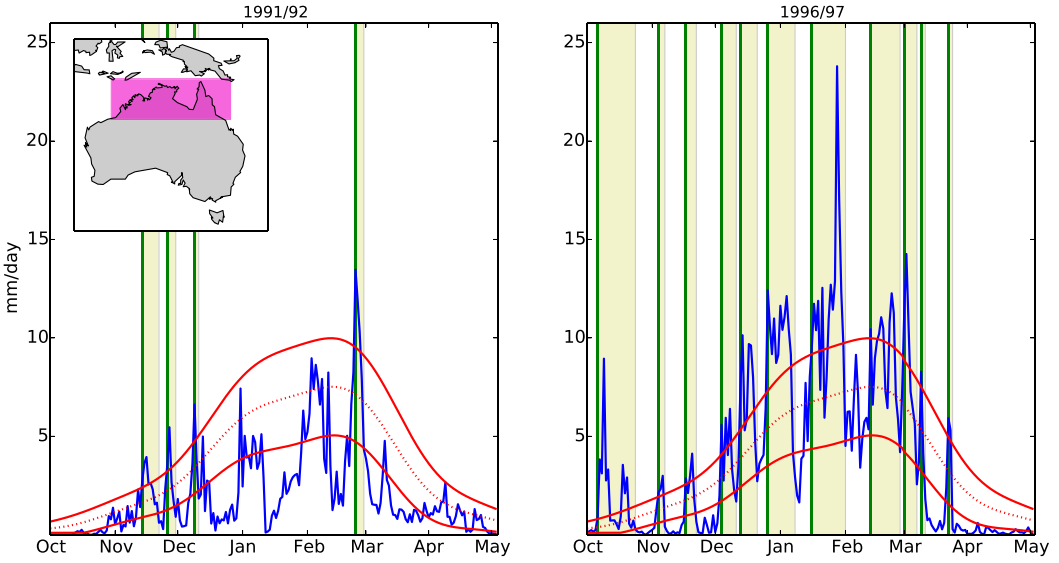

FIG. 1. The daily climatology of north Australian rainfall over land in the region 10°–20°S, 120°–150°E (see inset, shaded rectangle). The envelope defining below average and above average rainfall on any given day (red) shows the smoothed daily climatology ±0.5 standard deviation. Bursts (green) occur when rainfall changes from below average to above average in less than seven days as shown for two example wet seasons, (left) 1991/92 and (right) 1996/97 (blue). Each burst is deemed to last until rainfall has returned below the lower bound (light green shading).

Previous studies have exploited this relationship between absolute vorticity flux and circulation tendency to investigate the spin up of tropical cyclones (e.g., Raymond et al. 2014; Smith et al. 2015; Kilroy et al. 2016, 2017). The goal of the present study is to investigate the dynamics of Australian monsoon bursts, and in particular the transition from a break period to one with heavy rain. The net circulation is used to characterize the strength of the monsoon trough and determine the dynamical influences on monsoon bursts by investigating the vorticity fluxes leading to the circulation changes. For completeness we include an analysis of moisture flux changes during Australian monsoon bursts, and investigate how these changes are related to the net circulation in the monsoon region.

The remainder of this paper is structured as follows. The data and methodology are described in section 2. The meteorology of Australian monsoon bursts is examined and categorized in section 3. The physical mechanisms influencing Australian monsoon bursts are investigated in section 4. The key findings of this research are discussed in section 5, along with concluding remarks.

2. Data and methods

a. Data

The reference precipitation (daily) dataset used to diagnose monsoon bursts is from the Australian Water Availability Project (AWAP; Jones et al. 2009). This high-resolution dataset (0.05° × 0.05°) is chosen as it is based on the best available Australian rainfall observations for the north of Australia, and covers our study period (1979–2010).

The NOAA interpolated outgoing longwave radiation (OLR) dataset (resolution 2.5° × 2.5°) is used in this study (Liebmann 1996).

Wind, specific humidity, temperature, and mean sea level pressure data are taken from the European Centre for Medium-Range Weather Forecasts interim reanalysis (ERA-Interim; Dee et al. 2011). These reanalyses (resolution 0.75° × 0.75°) are provided at 6-hourly intervals but averaged to a daily interval to correspond with the AWAP rainfall dataset. Furthermore, vorticity and circulation are multiplied by −1, so that a positive change is cyclonic.

b. Burst composites

Following the method of Berry and Reeder (2016), rainfall over land is averaged over a box covering the north of Australia (10°–20°S, 120°–150°E), shown in Fig. 1. Using the daily time series from 1979 to 2010, a climatology is calculated for each day of the year. A climatology of the standard deviation in rainfall for each day of the year is also calculated. These climatologies are then smoothed using a low-pass filter that retains signals with periods longer than 60 days (i.e., the first six harmonics of the annual cycle). High and

low rainfall amounts are defined using the smoothed seasonal cycle, plus and minus half a smoothed standard deviation.

The beginning of a monsoon burst is then defined as the day on which northern Australian rainfall has increased from low rainfall (less than half a smoothed standard deviation below the smoothed average) to high rainfall (above half a smoothed standard deviation above the smoothed average), within a 7-day period. A burst is deemed to end when rainfall returns to below the low rainfall threshold given above. Bursts are defined to occur only during the northern Australian wet season (i.e., October–April). Bursts identified during two different wet seasons are presented as examples in Fig. 1. As seen in the figure, the method captures bursts throughout the wet season although there are some rainfall events that are not captured (e.g., February 1992). Most importantly, it provides a method to objectively define a monsoon burst. It should be noted that our burst definition pertains specifically to the sharp transition from break period to active rainfall. This differs from previous definitions that require a rainfall accumulation threshold in their burst criteria (e.g., Troup 1961; Wheeler and McBride 2005; Drosdowsky 1996). Although this has some limitations with regards to explaining total rainfall volumes in the wet season, this choice is made deliberately as it allows the dynamical influence on burst initiation throughout the wet season to be investigated.

Using the identified dates of the initiation of a burst, the average meteorological conditions leading up to the beginning of a burst are investigated. Variables of interest, including mean sea level pressure (MSLP), wind, temperature, and specific humidity, are averaged at the time of the beginning of the individual bursts. In some circumstances the anomaly of a variable can provide more insight, particularly when compositing variables with large seasonal variations that might mask any signal. For example, upper-level winds are very much affected by the seasonal transitions of the jet streams, and therefore composites of meridional wind anomalies are more useful for identifying Rossby wave activity. To calculate the anomalous values of a variable we calculate first a smoothed annual cycle in the same manner described above for rainfall. The anomaly for each day of the year is then simply the deviation of that variable from its mean value for that day of the year.

Although the appropriateness of significance testing is arguable (e.g., Nicholls 2001; Johnson 1999; Gill 1999) we provide it here for completeness. The statistical significance of field anomalies is determined using the Student's t test.

3. The meteorology of Australian monsoon bursts

a. Circulation tendency

The Eulerian vertical vorticity tendency equation in isobaric coordinates is

$$\frac{\partial \zeta_p}{\partial t} = -\nabla \cdot \mathbf{Z}, \tag{1}$$

where

$$\mathbf{Z} = \mathbf{u}_h \zeta_a - \omega \boldsymbol{\zeta}_h + \mathbf{k} \wedge \mathbf{F}_{\text{fri}}. \tag{2}$$

In Eq. (2), $\mathbf{Z}$ is the horizontal flux of absolute vorticity (m s^{-2}), ζ_p is the vertical component of relative vorticity (s^{-1}), $\mathbf{u}_h$ is the horizontal velocity vector (m s^{-1}), ζ_a is the vertical component of absolute vorticity (s^{-1}), ω is the vertical velocity in pressure coordinates (Pa s^{-1}), $\boldsymbol{\zeta}_h$ is the horizontal vorticity vector in pressure coordinates (m Pa s^{-1}), $\mathbf{k}$ is the unit vector in the vertical direction, and $\mathbf{F}_{\text{fri}}$ is the frictional force per unit mass (m s^{-2}). The three terms in Eq. (2) sequentially represent the advective flux of absolute vertical vorticity, the vorticity flux associated with vortex tilting, and finally a vorticity flux associated with friction. The third term is assumed to be relatively small and is therefore neglected in this study. Equation (1) states that the vertical vorticity in a bounded region can only change by the horizontal convergence of absolute vorticity flux (Haynes and McIntyre 1987).

The circulation Γ around a closed circuit can be related to vorticity using Stokes theorem, so that

$$\Gamma = \int_C \mathbf{u} \cdot d\mathbf{x} = \int_A \zeta_p \, dA, \tag{3}$$

where C is the closed circuit around the region A, and $\mathbf{u}$ is the velocity vector. Combining Eqs. (3) and (1) and applying the two-dimensional divergence theorem, we obtain the circulation tendency equation:

$$\frac{d\Gamma}{dt} = -\oint_C \mathbf{Z} \cdot \hat{\mathbf{n}} \, dS, \tag{4}$$

where $\hat{\mathbf{n}}$ is the unit outward normal along the path C. Equation (4) simply states that the net circulation change in a region bounded by the curve C is equal to the normal component of absolute vorticity flux integrated along the closed path of C.

It is important to note that the influence of convection on circulation tendency is implied in Eq. (2) by the vertical flux of horizontal vorticity term $\omega\boldsymbol{\zeta}_h$, which results in dipoles of cyclonic and anticyclonic vorticity. If the convection is confined within the closed region this

does not affect the net circulation. Thus, circulation only changes by the convergence of absolute vorticity flux through the boundaries of the closed region. In this way, it is the concentration of vorticity which leads to the amplification of circulation.

We now apply the circulation tendency equation to the strengthening of the monsoon trough at the start of heavy rainfall with the aim of inferring the key influences on the initiation of Australian monsoon bursts. There is likely to be feedback between circulation and precipitation; however, for circulation to increase there must be convergence of vorticity flux. By investigating the physical mechanisms leading to circulation changes, we hope to explain the observed changes in precipitation.

We begin our investigation by creating a time-lag composite of the daily anomaly of the terms in Eq. (4) around rainfall burst days, with day 0 marking the beginning of the composite burst (Fig. 2). Four days before the start of the burst, there is an anticyclonic circulation tendency anomaly below approximately 800 hPa. On the day of the composite burst, the circulation tendency anomaly in the monsoon region has become cyclonic through a deep layer (below 650 hPa). This is largely the result of an increase in the convergence of planetary vorticity flux, while changes to the convergence of relative vorticity flux and the convergence of tilted horizontal vorticity flux are minor. Even in the absence of relative vorticity flux, the stretching or advection of planetary vorticity leads to a cyclonic increase in circulation.

Figure 3 shows the lag composite of column-integrated low-level (from 850 to 1000 hPa) convergence of absolute vorticity flux anomaly into the monsoon region. The flux has been separated according to the boundary at which the absolute vorticity enters the monsoon region (north, east, south, or west). As seen in Fig. 2 there is a rapid increase in the convergence of absolute vorticity flux anomaly (Fig. 3) prior to the beginning of the rainfall burst. As the beginning of the burst approaches, the anomalous flux of absolute vorticity through of the southern boundary (negative) reverses direction (into the region and positive), which leads to a rapid increase of cyclonic circulation about the region. The anomalous vorticity flux through the western and northern boundaries increases slightly over the onset of the burst, while the anomalous vorticity flux through the eastern boundary decreases.

Monsoon break periods are associated with easterly flow (Pope et al. 2009), and so it is unsurprising that there is an easterly vorticity flux anomaly prior to the start of the burst. Most of the change in circulation associated with the initiation of the burst can be attributed to the change in sign of vorticity flux at the southern boundary.

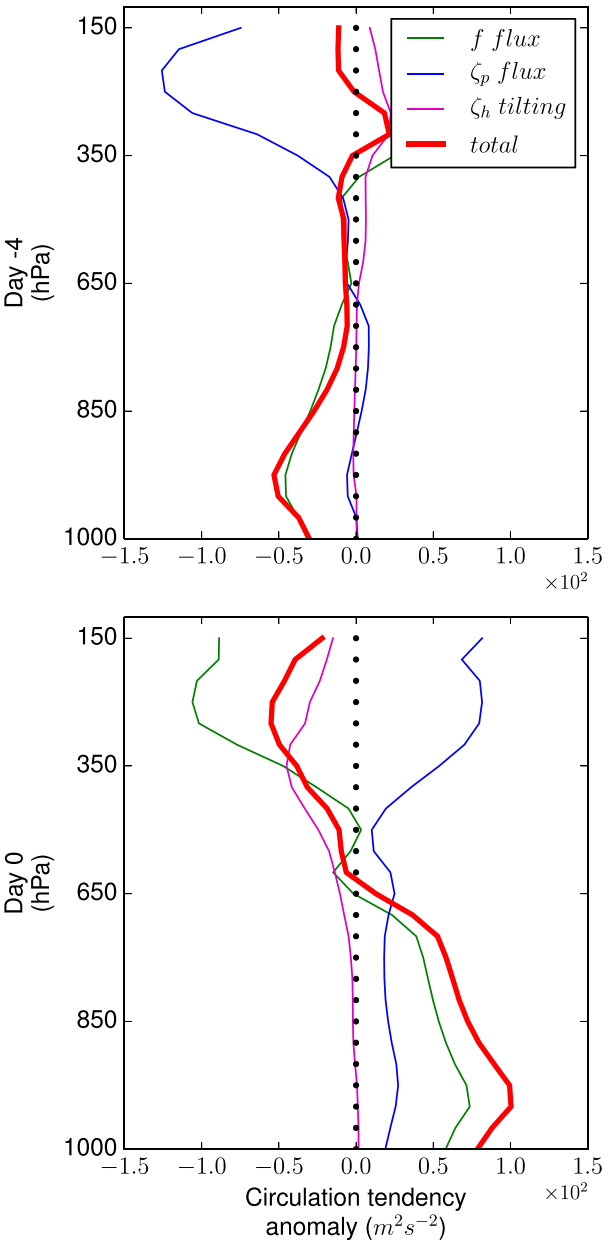

FIG. 2. Lag composite vertical profiles of circulation tendency anomaly ($10^2\,m^2\,s^{-2}$, thick red) and its components in the Australian monsoon region at burst days (top) −4 and (bottom) 0; ζ_p flux is the flux of the vertical component of relative vorticity (blue), f flux is the flux of the vertical component of planetary vorticity (green), and $\boldsymbol{\zeta}_h$ tilting is the vorticity flux due to the tilting of the horizontal component of relative vorticity (magenta).

b. *Moisture flux convergence*

The column-integrated (from 1 hPa to the surface) Eulerian specific humidity q tendency equation is

$$\frac{\partial}{\partial t}\int_A q\,dA = -\oint_C (\mathbf{u}_h q)\cdot\hat{\mathbf{n}}\,dS + \int_A (E-P)\,dA, \quad (5)$$

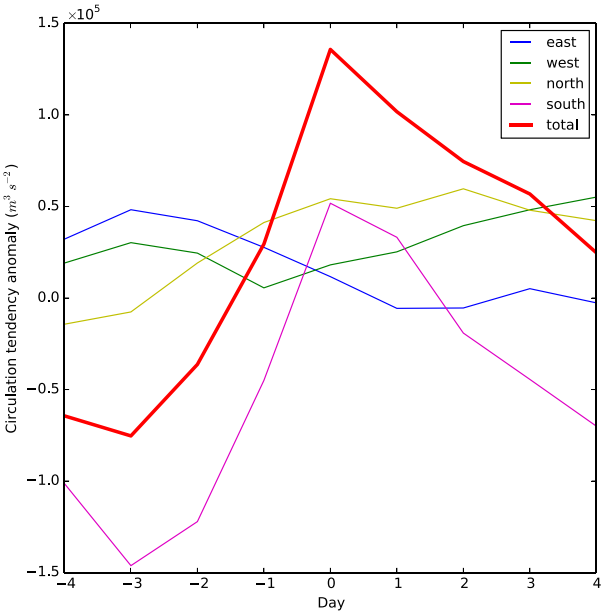

FIG. 3. Lag composite of column-integrated (from 1000 to 850 hPa) absolute vorticity flux anomaly ($10^3\,m^3\,s^{-2}$) into the monsoon region from the east (blue line), west (green line), north (yellow line), and south (magenta line), and the circulation tendency anomaly, which is the sum of the fluxes across all boundaries (thick red line).

where $E - P$ is the difference between evaporation and precipitation. The terms on the right-hand side represent horizontal moisture flux convergence and the moisture source terms (evaporation minus precipitation), respectively. By column integrating the moisture budget we remove the vertical moisture flux term, since there is no moisture flux at the top and bottom of the atmosphere except the source terms.

The lag composite of moisture flux convergence anomaly in the Australian monsoon region is shown in Fig. 4. Four days prior to the burst there is an anomalous divergence of moisture below approximately 700 hPa. By the day of the burst there is a strong moisture flux convergence anomaly through a deep layer over the region.

Figure 5 shows the lag composite of column-integrated (1000–1 hPa) moisture flux convergence anomaly into the monsoon region, which has been decomposed into the moisture flux through each of the monsoon region boundaries. The change in column-integrated specific humidity is equal to the sum of moisture flux convergence and the source term, which is evaporation minus precipitation. The evaporative flux, estimated from the surface latent heat flux, remains almost constant over the course of the burst (not shown). The precipitation in the region, by definition, increases at the start of the burst.

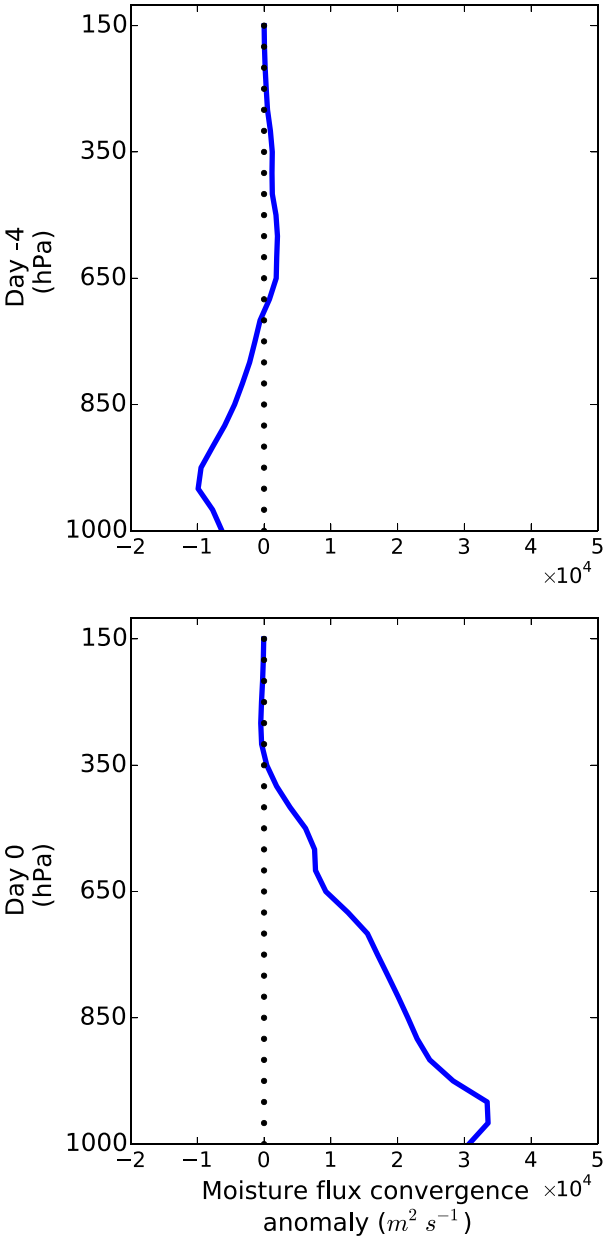

FIG. 4. Lag composite vertical profiles of moisture flux convergence anomaly ($10^4\,m^2\,s^{-1}$) into the Australian monsoon region at burst days (top) −4 and (bottom) 0.

The total moisture flux convergence anomaly steadily increases from three days prior to the burst, peaking at the beginning of the burst (day 0). The moisture flux anomaly through the eastern boundary is the main source of moisture for the region prior to the start of the burst, although it steadily decreases as the burst progresses. The moisture flux anomalies through the western and northern boundaries both change from negative prior to the burst to slightly positive after the beginning of the burst. The moisture flux anomaly through the

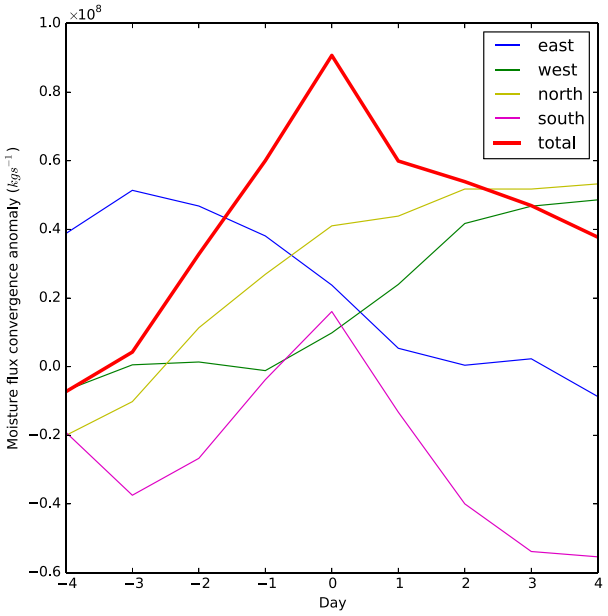

FIG. 5. As in Fig. 3, but for the lag composite of column-integrated (1000–1 hPa) moisture flux convergence anomaly (10^8 kg s^{-1}).

southern boundary is also negative at three days prior to the burst; however, it becomes positive coinciding with the start of the burst and then becomes negative again after the burst commences. The decrease in moisture loss through the northern, western, and southern boundaries leads to an accumulation of moisture in the region prior to the start of the burst.

c. *Relating circulation and moisture changes*

Figure 6 shows the scatterplot of moisture flux convergence against circulation tendency for all wet season days (Fig. 6, top) and on the day of the monsoon bursts (Fig. 6, bottom). The shading indicates the rainfall on that day. The rainfall appears to be proportional to the moisture flux into the region for both the entire wet season as well as for the burst cases. From the wet season plot (Fig. 6, top) it can be seen that low (or negative) moisture flux convergence corresponds to lower rainfall. There are a few days with rainfall exceeding 12 mm during the wet season that have an anticyclonic change in circulation and a small or negative moisture flux convergence. These cases were found to correspond to tropical cyclones or tropical depressions near the northwest coast of Australia that subsequently tracked out of the monsoon region along the west coast (not shown).

The relationship between circulation tendency and moisture flux convergence appears to be similar for monsoon bursts (Fig. 6, bottom). Large cyclonic circulation changes frequently correspond to large moisture

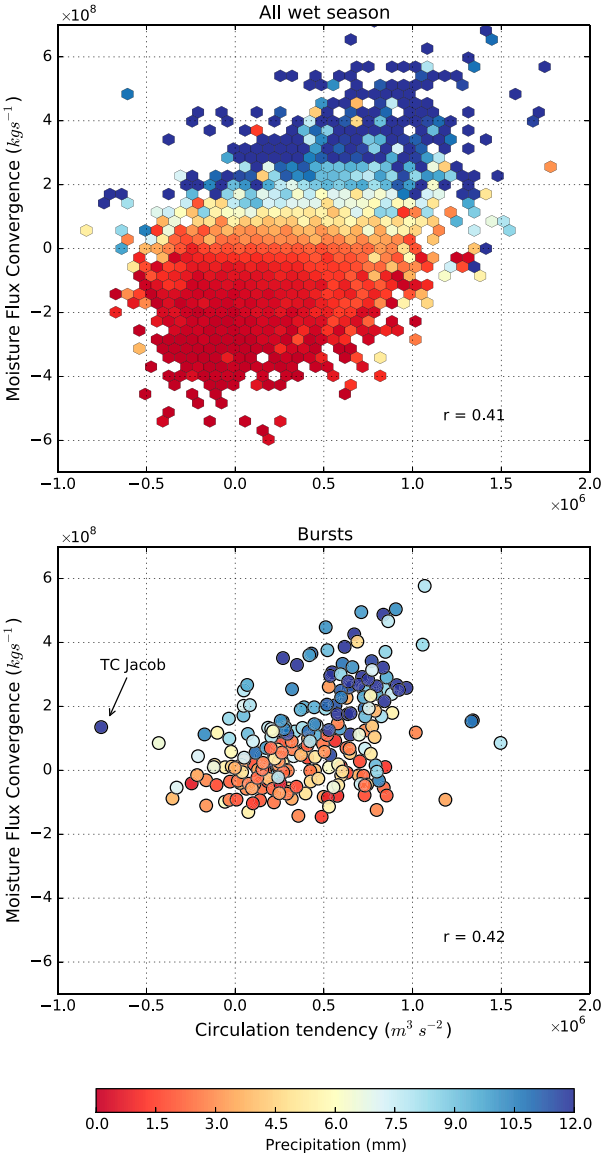

FIG. 6. Column-integrated (from 1000 to 1 hPa) moisture flux convergence (10^8 kg s^{-1}) vs column-integrated (from 1000 to 850 hPa) absolute vorticity flux convergence (circulation tendency; 10^6 m^3 s^{-2}) for (top) the whole wet season and (bottom) the day of bursts. The shading is scaled according to the amount of precipitation on that day. The wet season is shaded according to the mean value of precipitation in each hexagon. A positive flux is defined as into the monsoon region. The absolute vorticity flux is scaled by −1, so that a positive value is associated with an increase in cyclonic circulation in the monsoon region.

flux convergence and larger rainfall. In fact, more than 80% of northern Australian rainfall occurs on a day where the circulation tendency is cyclonic. One exception to this relationship, Tropical Cyclone Jacob, is annotated in Fig. 6, bottom. This cyclone made landfall in early March 2007 on the northwest coast of Australia,

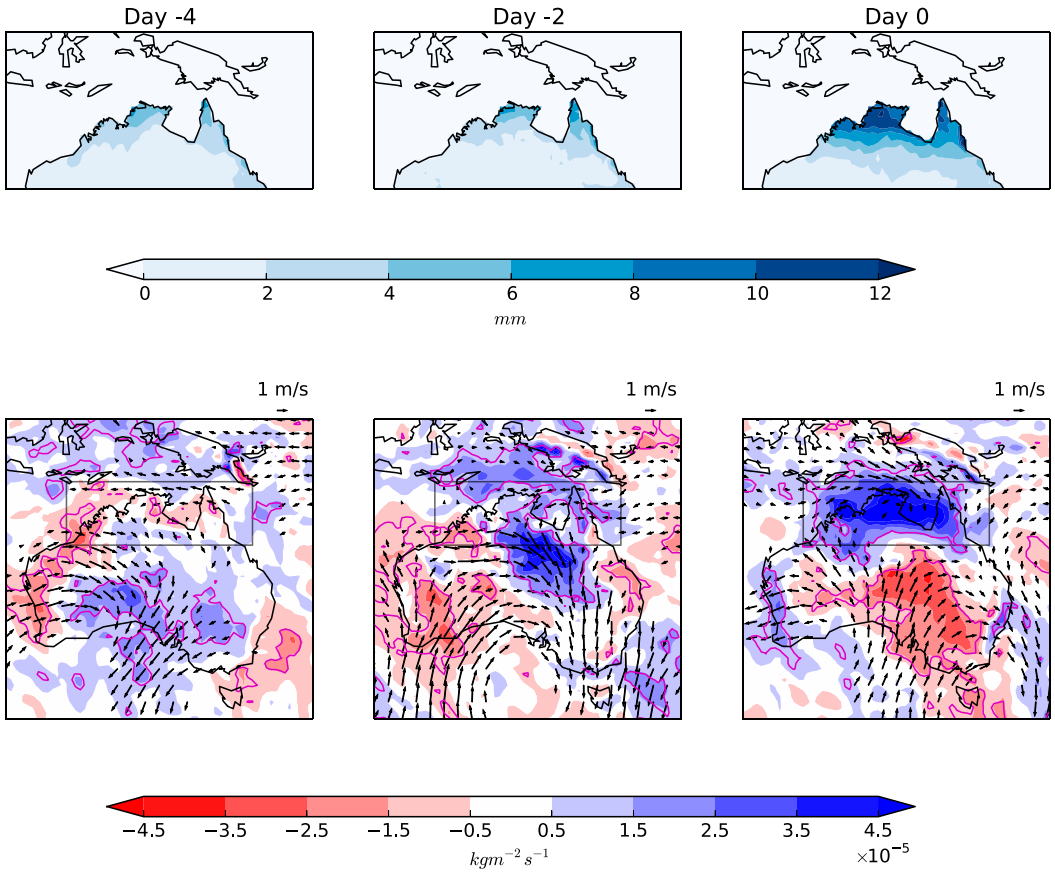

FIG. 7. Burst mean lag composite (at days −4, −2, and 0) of (top) daily precipitation (mm) and (bottom) column-integrated (from 1000 to 1 hPa) moisture flux convergence anomaly (10^{-5} kg m^{-2} s^{-1}), with 950-hPa wind anomaly vectors. The black box in (bottom) marks the monsoon region boundary. Wind anomalies are only plotted where they are significant above the 95% level. Magenta contours indicate field anomalies that are significant above the 95% level.

and subsequently progressed southward out of the monsoon region. It caused localized heavy precipitation within the region of investigation (inset in Fig. 1) and a strong anticyclonic change in circulation as the cyclone left the region. The net moisture flux convergence was positive, although relatively small compared to other heavy rainfall burst events.

To better understand the spatial organization of moisture flux convergence anomalies, we show lag composite maps in Fig. 7 (bottom), along with 950-hPa wind anomaly vectors. Four days prior to the burst there is moisture flux divergence throughout much of the monsoon region. Wind anomaly vectors in the monsoon region are predominantly easterly. Two days prior to the burst a cyclonic wind anomaly is prevalent over the Great Australian Bight, and a positive moisture flux convergence anomaly is found at the northeastern edge of the cyclonic wind anomaly (to the south of the monsoon region). The wind anomaly vectors at the southern boundary of the monsoon region reveal an export of moisture out of the region. On the day of the burst there is a positive moisture flux convergence anomaly throughout the monsoon region. The midlatitude cyclonic anomaly has moved farther toward the southeast. At the southern boundary the wind anomaly vectors are either pointing into the monsoon region, or are parallel with the boundary. A cyclonic wind anomaly pattern has formed in the monsoon region, indicative of the increased cyclonic circulation (cf. Fig. 3) and an active monsoon trough.

d. Convective instability

The transition from break period to burst marks a rapid increase in deep convection in the monsoon region. We investigate the strength of convective instability during the burst transition using the modified K index (Charba 1977). It is defined as

$$K = \frac{T_{\text{sfc}} + T_{850}}{2} - T_{500} + \frac{T_{d_{\text{sfc}}} + T_{d_{850}}}{2} - T_{700} + T_{d_{700}}, \quad (6)$$

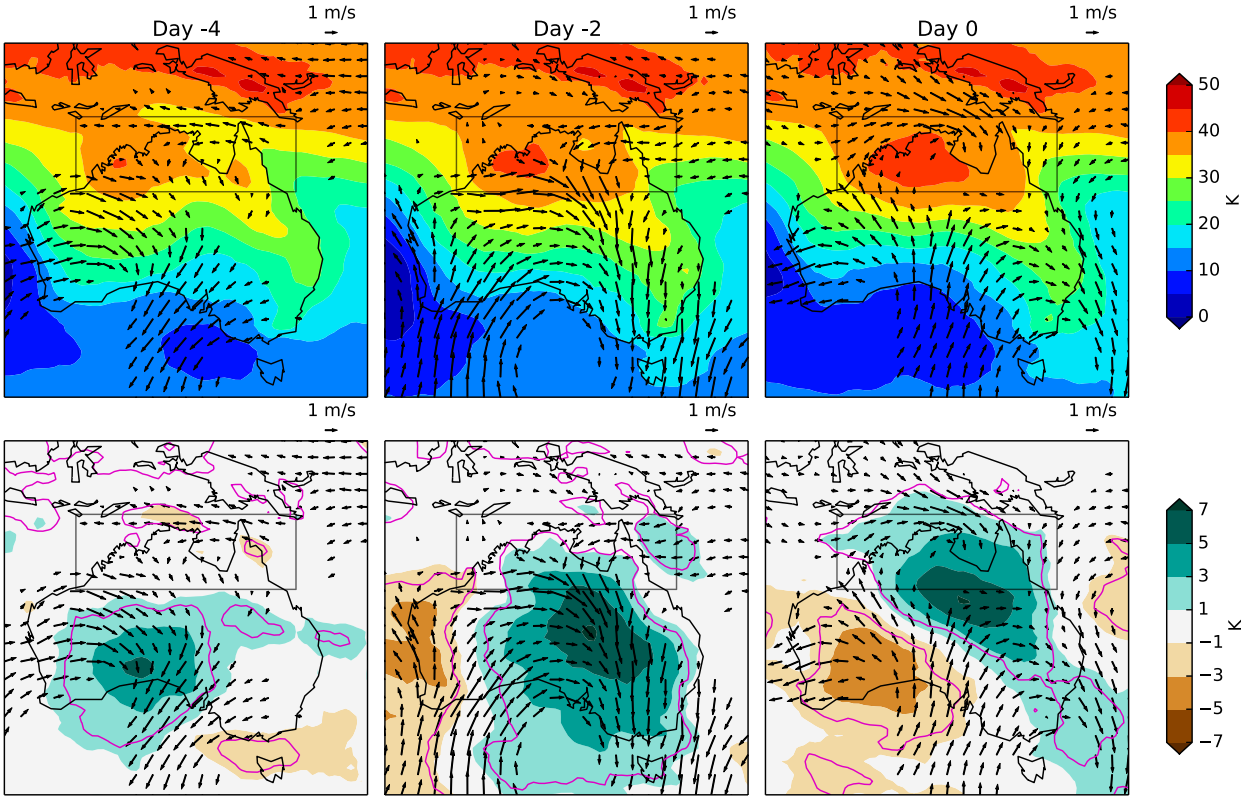

FIG. 8. Burst mean lag composite (at days −4, −2, and 0) of (top) *K* index (K) and (bottom) *K* index anomaly (K), with 950-hPa wind anomaly vectors. The black box marks the monsoon region boundary. Wind anomalies are only plotted where they are significant above the 95% level. Magenta contours indicate field anomalies that are significant above the 95% level.

where T_p and T_{d_p} are the temperature and dewpoint temperature at pressure p (hPa), and the subscript sfc indicates the surface value of the field. The *K* index is commonly used to predict deep convection and thunderstorm activity, and has been used in several studies as a measure of convective instability (e.g., Tan et al. 2013). It is a relatively simple measure of convective instability, and is chosen in part due to its suitability to the gridded reanalysis data used in this study.

Figure 8 shows the lag composite of *K* index (Fig. 8, top) and *K* index anomalies (Fig. 8, bottom) with 950-hPa wind anomaly vectors. Larger values of the *K* index indicate increased convective instability.

Four days prior to the burst, the western part of the monsoon region has *K* index values between 35 and 40 K, while the east of the monsoon region has values less than 35 K. The *K* index anomaly is positive over the southwest of Australia, at the northeastern edge of the midlatitude cyclonic anomaly. Two days prior to the burst the convective instability has increased over most of the monsoon region, with *K* index values greater than 35 K, and a peak over the northwest of Australia greater than 40 K. The midlatitude positive *K* index anomaly has strengthened and shifted over the continent. A negative *K* index anomaly is found to the northwest of the cyclonic wind anomaly, indicating stable or subsiding conditions. On the day of the burst the *K* index is above 40 K over a broad area covering the western and central parts of the monsoon region. There is a positive *K* index anomaly throughout much of the monsoon region, extending through the southern boundary of the monsoon region.

The increase in convective instability prior to the burst appears to be largely driven from the south of the monsoon region.

e. *Categorizing bursts*

The lag composite of circulation tendency (Fig. 3) suggests that the transition from break period to burst is characterized by the change in vorticity flux through the southern boundary. Figure 9 shows the distribution of the correlation of circulation tendency and absolute vorticity flux through each boundary of the monsoon region, for all individual monsoon bursts. The correlation is calculated using a sample of five days around each burst. The distributions of the

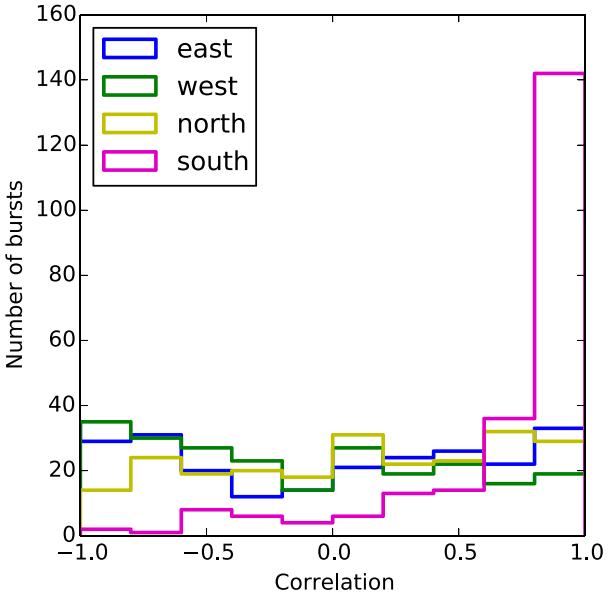

FIG. 9. Histogram of the correlation between circulation tendency and absolute vorticity flux through each boundary of the monsoon region for all individual burst events.

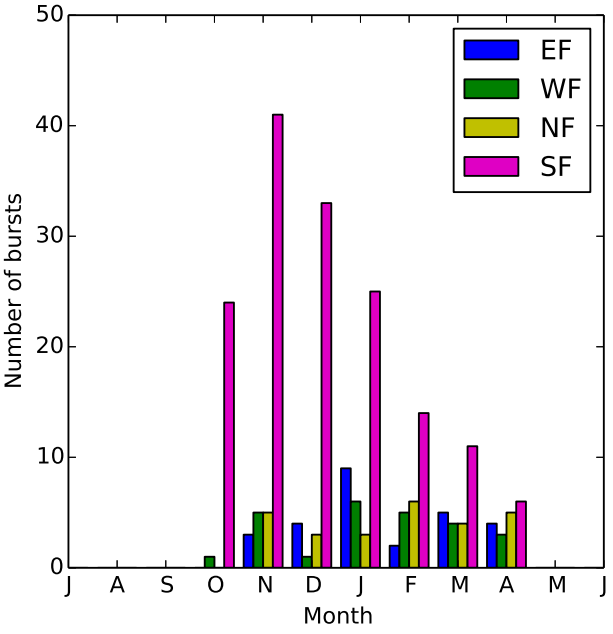

FIG. 10. The occurrence of bursts in each month of the year, categorized by the direction of absolute vorticity flux with greatest influence on circulation tendency. Bursts with greatest influence from the south are referred to as SF-influenced bursts (magenta), and similarly for NF- (yellow), EF- (blue), and WF-influenced (green) bursts.

correlation between the circulation tendency and the absolute vorticity flux through the northern, western, and eastern boundaries are all approximately uniform. The distribution of correlation between the circulation tendency and the absolute vorticity flux through the southern boundary is heavily skewed toward a high positive correlation. This high positive correlation indicates that the changes in vorticity flux through the southern boundary are important for burst initiation.

Given the likely special role of vorticity flux through the southern boundary, we now categorize each burst according to the boundary that contributes most to the change in the circulation. To do this, we identify the boundary whose vorticity flux correlates best with the total circulation change. For example, bursts with the largest correlation between circulation tendency and absolute vorticity flux through the southern boundary will hereafter be referred to as "southerly flux" (SF)-influenced bursts.

The occurrence of the four burst categories is shown in Fig. 10. The SF category is the most numerous in all months of the wet season (154 out of the total 232 events), although it shows a strong seasonality with a peak in November and decreasing throughout the wet season, consistent with the results of Berry and Reeder (2016). The northerly (NF), easterly (EF), and westerly flux (WF) categories have much smaller sample sizes; however, the numbers of NF, EF, and WF bursts combined appear to peak between January and March, which broadly coincides with the peak of wet season rainfall (see Fig. 1).

Figure 11 shows the normalized distribution of rainfall for the first three days of each burst for both the SF

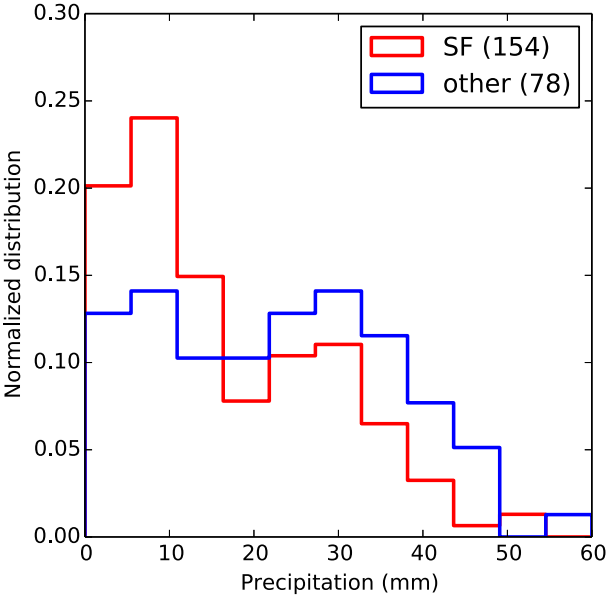

FIG. 11. Normalized distribution of burst precipitation accumulated for the first three days of each burst. The normalized distribution is plotted for the SF burst category (red) and for all other bursts combined (blue).

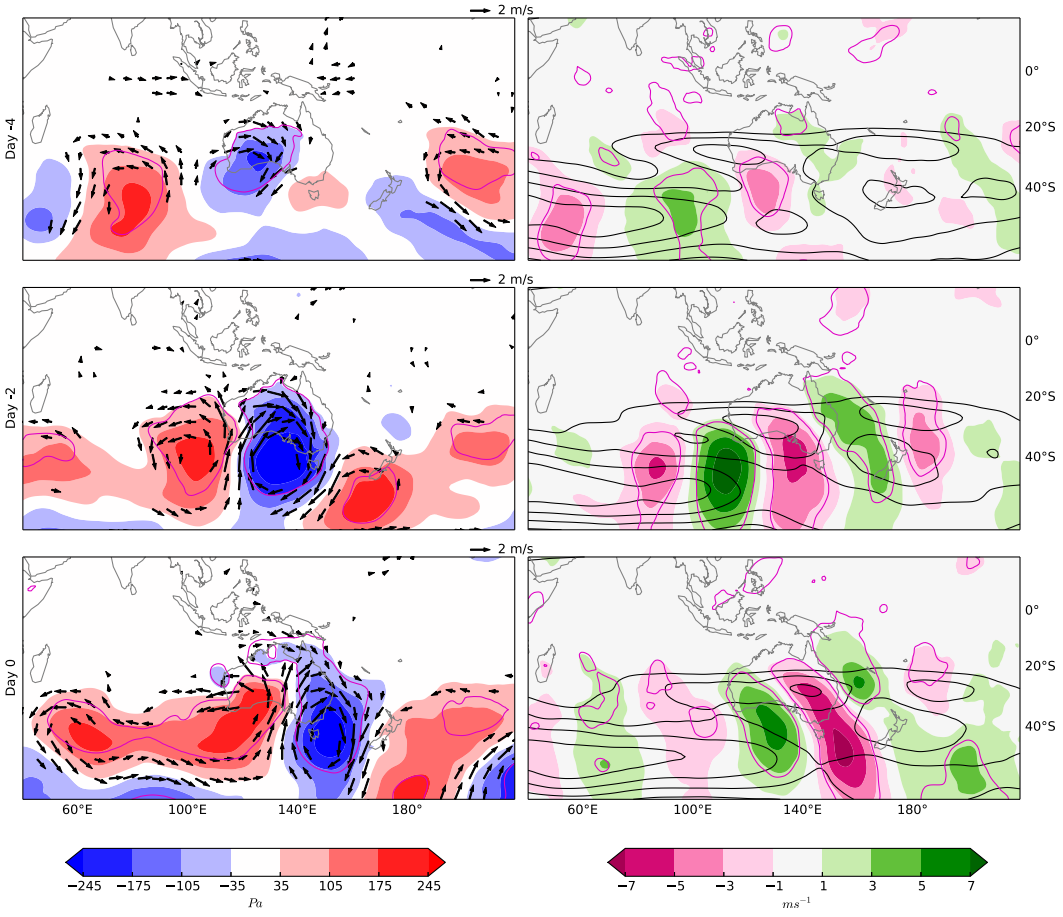

FIG. 12. Lag composites of (left) MSLP anomaly (Pa) with 950-hPa wind anomaly vectors and (right) 200-hPa meridional wind anomaly with 200-hPa zonal wind contours (starting from 20 m s^{-1}, with intervals of 10 m s^{-1}) at days (top) −4, (middle) −2, and (bottom) 0, of SF events. Wind anomalies are only plotted where they are significant above the 95% level. Magenta contours indicate field anomalies that are significant above the 95% level.

bursts, and the collection of all other bursts. The SF bursts have a distribution slightly more skewed toward lower rainfall; however, given their greater frequency in the premonsoon period (October–November) this result is unsurprising. SF-related rainfall (i.e., days where circulation tendency is most strongly correlated with the southern boundary vorticity flux) accounts for approximately 60% of the total wet season rainfall. Since the SF bursts comprise two-thirds of all bursts and are related to much of the wet seasons rainfall, they are clearly important. The following section will therefore focus on SF bursts.

4. The key physical mechanisms of Australian monsoon bursts

a. *A midlatitude influence*

Figure 12 shows lag composite maps of MSLP anomaly (Fig. 12, left) as well as the 200-hPa meridional wind anomaly (Fig. 12, right), for all SF bursts. Four days prior to the burst (Fig. 12, top) a cyclonic anomaly appears over the southwest of the Australian continent. To the southwest of Australia, an anticyclonic anomaly is present over the southern Indian Ocean (approximately 50°S, 80°E). Two days later (i.e., day −2; Fig. 12, middle), the cyclonic anomaly over the continent strengthens and moves slightly eastward, with its center over the Great Australian Bight. The cyclonic anomaly extends over most of the continent. Anticyclonic anomalies lie both ahead of and behind the cyclonic anomaly, forming a wavelike pattern. In the midlatitudes (centered around 40°S) at upper levels, the meridional wind anomalies exhibit a wavelike pattern also, with a northerly anomaly over the continent and southerly anomalies on either side two days prior to the burst (Fig. 12, middle). This configuration corresponds to an upper-level anticyclone over the east coast of Australia, with an upper-level cyclone to the west. In combination with the MSLP anomalies, there

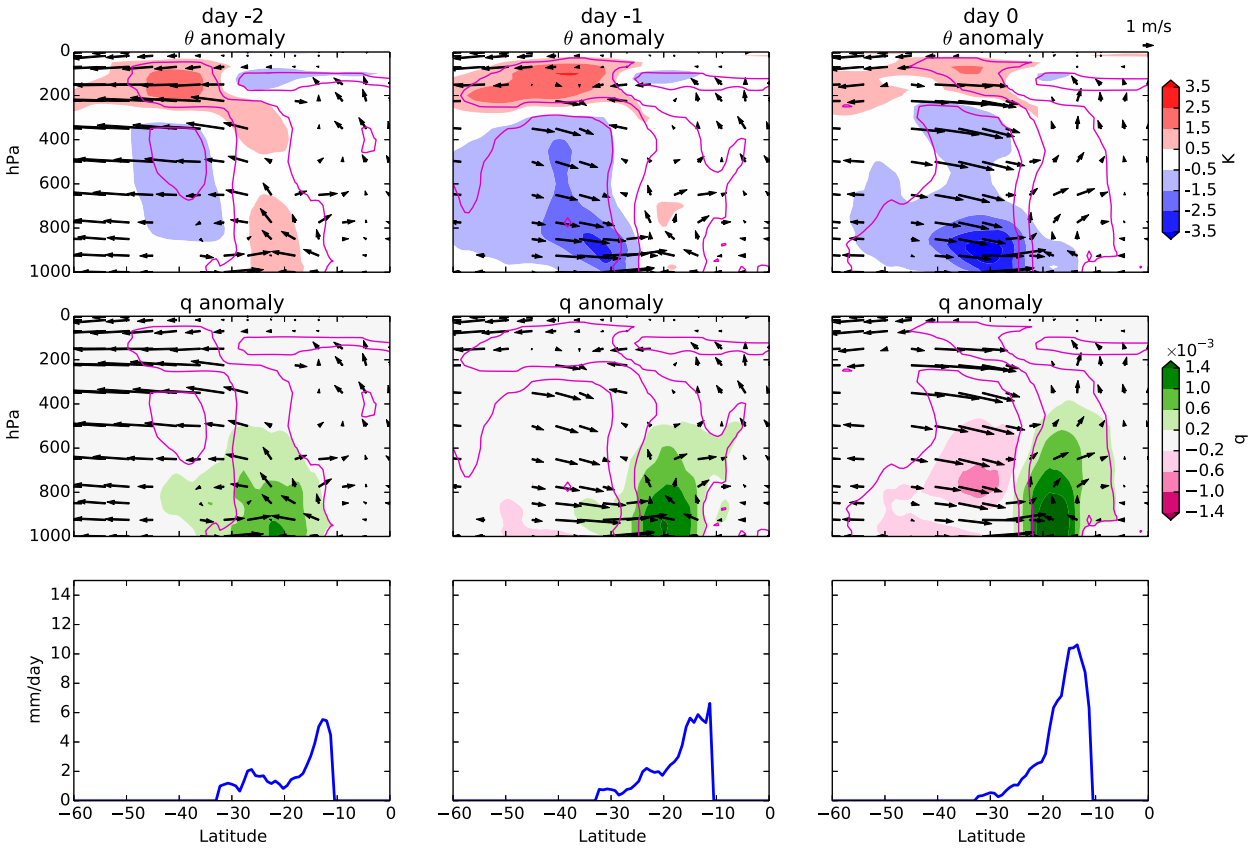

FIG. 13. Lag composites at day (left) −2, (center) −1, and (right) 0, along a cross section from 60°S to the equator, through Darwin (130°E). (top) Potential temperature anomaly (K) and meridional and vertical wind speed vectors ($m\,s^{-1}$). The vertical wind component has been scaled by a factor of 100. (middle) Specific humidity anomaly ($10^{-3}\,kg\,kg^{-1}$) with the same wind vectors as in (top). (bottom) Precipitation ($mm\,day^{-1}$) along the cross section. Wind anomalies are only plotted where they are significant above the 95% level. Magenta contours indicate field anomalies that are significant above the 95% level.

appears to be a westward-tilting wave structure. The cyclonic anomaly (stretching from approximately 50°S to nearly 20°S) provides an extratropical influence, with northerly flow out of the monsoon region at the eastern edge of the cyclonic anomaly, and southwesterly flow into the monsoon region on the western edge of the cyclonic anomaly.

On the day of the burst (Fig. 12, bottom), the cyclonic anomaly has contracted over the east coast of Australia, with the trough extending toward the monsoon region. The anticyclonic anomaly to the west of it has expanded over the continent. The composite of upper-level zonal winds show a strong subtropical jet over the continent, which does not change substantially after the commencement of the composite of SF bursts. This result is very similar to the composite of all monsoon bursts, shown by Berry and Reeder (2016), although they found that the subtropical jet was not essential for the occurrence of monsoon bursts. It is clear that the SF burst category is associated with a midlatitude Rossby wave, and its associated low-level trough.

A north–south vertical cross section through the Australian continent near Darwin (from 60°S to the equator, at 130°E) is shown in Fig. 13 to assess the SF bursts further. Two days prior to the burst an upper-level (200 hPa) positive temperature anomaly is present above a negative temperature anomaly (from 400 to 850 hPa) in the midlatitudes (near 40°S; see Fig. 13, top center). This dipole pattern is representative of an upper trough. There is a negative specific humidity anomaly (Fig. 13, middle) at low levels equatorward of the negative temperature anomaly. This low-level moistening is the result of low-level moisture flux convergence (as shown in Fig. 5). The wind vectors indicate a shallow overturning circulation equatorward of 10°S. Rainfall in the monsoon region is less than $6\,mm\,day^{-1}$.

On the day before the burst the negative temperature anomaly from the midlatitudes has shifted equatorward,

primarily at low levels (below 700 hPa). The southerly wind vectors over the Australian continent (between 20° and 40°S) are consistent with flux of planetary vorticity through the southern boundary of the monsoon region and the subsequent increase in cyclonic circulation (seen in Fig. 3). The specific humidity anomaly has increased further as a result of moisture advection ahead of the trough.

On the day of the burst, the negative temperature anomaly from the midlatitudes has moved northward over the continent, with the frontlike boundary (between 10° and 20°S) weakening (Fig. 13, top right). There is a deep layer of strong southerly winds (from the surface to 200 hPa) between 20° and 40°S. Rising motion is found in a deep layer (from the surface to 200 hPa) throughout the entire monsoon region (10°–20°S).

Ahead of the frontlike structure, the increased moisture flux convergence has led to a positive moisture anomaly in a deep layer up to about 500 hPa (Fig. 13, middle right). The peak precipitation in the monsoon region has increased to more than 10 mm day^{-1} (Fig. 13, bottom right).

The vertical cross section composites provide a complementary view of the midlatitude influence on burst initiation seen in the MSLP and upper-level winds (Fig. 12). Ahead of the trough moisture converges into the monsoon region. As the trough reaches the monsoon region the rainfall burst is initiated. The transition from break period to burst is further investigated through composites of the OLR anomaly, which is often used as an indicator of deep convective clouds. The lag composite of OLR for all SF bursts is shown in Fig. 14 (color shading), with low-level wind vector anomalies. Four days prior to the composite burst, a positive OLR anomaly covers much of tropical north Australia, consistent with the suppressed conditions during monsoon breaks. Wind anomalies over the north of Australia are small (less than 1 m s^{-1}) but predominantly easterly. Over most of the Maritime Continent to the north of Australia, a weakly negative OLR anomaly exists, with a positive anomaly lying over the western Pacific equatorial region (near 180°). Over the southwest of Australia and the Australian Bight there is a negative OLR anomaly associated with a low-level cyclonic anomaly (30°S, 120°E). To the west of the cyclonic anomaly is a series of anticyclonic and cyclonic wind anomalies, indicative of the midlatitude wave pattern.

Two days prior to the burst there is a negative OLR anomaly over the Maritime Continent and a positive OLR anomaly over the western Pacific. The positive OLR anomaly over the north of Australia has moved equatorward. The negative anomaly over the southwest of Australia has shifted northeastward toward the monsoon region, while the cyclonic wind anomaly over the continent has also shifted northeastward and strengthened. The midlatitude wave pattern over Australia is clearly visible in the low-level wind anomalies.

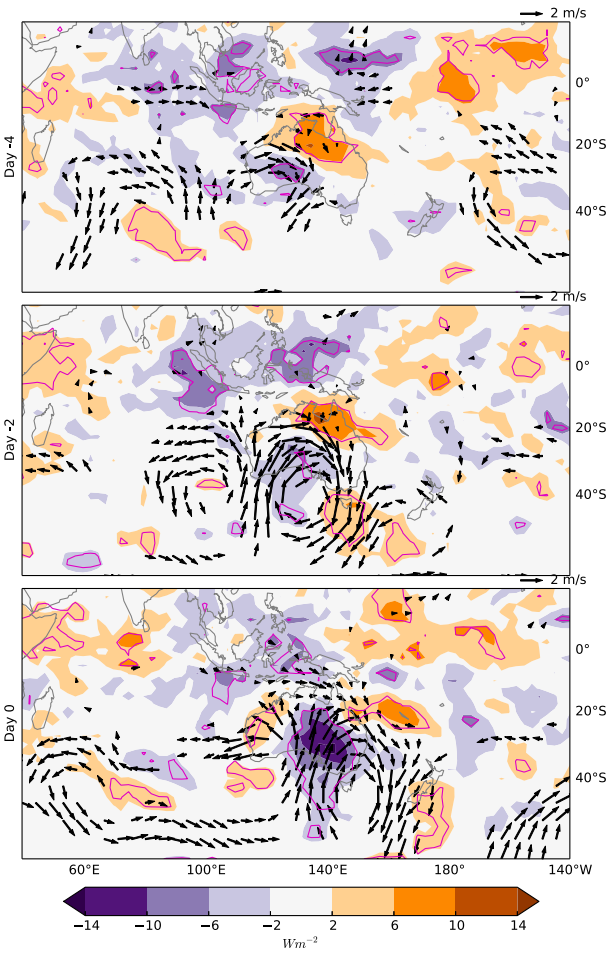

FIG. 14. Lag composites of OLR (W m^{-2}) at days (top) −4, (middle) −2, and (bottom) 0, of SF events. OLR anomaly is shown in color shading, and the wind vectors are at 950 hPa (reference vector shown at top right in each panel). Wind anomalies are only plotted where they are significant above the 95% level. Magenta contours indicate field anomalies that are significant above the 95% level.

On the day of the burst, the negative OLR anomaly over the continent has strengthened, with a northwest–southeast tilt, typical of a midlatitude trough. Strong southerly winds between the cyclonic and anticyclonic wind anomalies advect extratropical air into the monsoon region (between 110° and 150°E). The positive OLR anomaly over the north of Australia has shifted offshore and westerly wind anomalies prevail over much of the monsoon region. The weak negative OLR anomaly over the Maritime Continent has persisted and has extended toward the Gulf of Carpentaria.

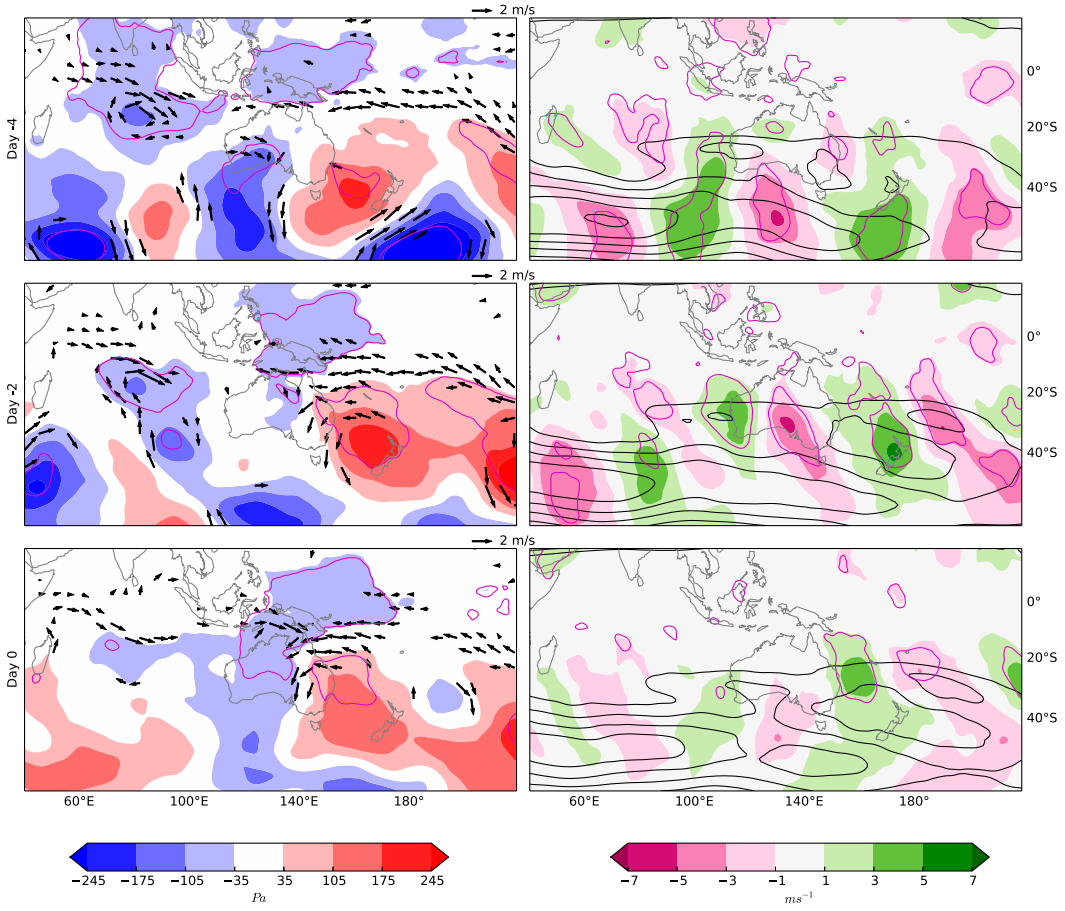

FIG. 15. As in Fig. 12, but for non-SF events (i.e., NF, EF, and WF).

The extratropical influence for SF monsoon bursts is clear. A midlatitude trough or front changes the sign of vorticity flux at the southern boundary of the region and, as a result, the circulation increases. Moisture converges in the monsoon region ahead of the midlatitude trough leading to a burst.

b. *Non-SF bursts*

Having investigated the SF burst structure, we now turn our attention to the remaining one-third of the burst events. Figure 15 shows the lag composite of MSLP anomaly for all non-SF bursts (i.e., EF, WF, and NF bursts). Four days prior to the burst (Fig. 15, top) a series of high and low MSLP anomalies stretch from 100°E to past 160°W, in the midlatitude region (around 40°S). A high pressure anomaly straddles the Tasman Sea, to the east of a low pressure anomaly extending to the south of Western Australia. Two days prior to the burst (Fig. 15, middle) the high pressure anomaly remains over the Tasman Sea, while the low pressure anomaly to the south of Western Australia has weakened. The upper-level meridional winds exhibit a wave pattern, implying an upper-level anticyclonic anomaly over the eastern seaboard and an upper-level cyclonic anomaly over the west of the continent. By the day of the burst (Fig. 15, bottom), the high pressure anomaly over the Tasman Sea has weakened. A north–south-oriented low pressure anomaly extends over the continent from 50°S toward the monsoon region, consistent with a weak midlatitude trough. The upper-level wave pattern in meridional wind has weakened. The midlatitude anomalies in the composite of the non-SF bursts are weaker than those in the composite of SF bursts.

The lag composite of OLR for all non-SF bursts (i.e., EF, WF, and NF bursts) is shown in Fig. 16, with low-level wind vector anomalies. Four days prior to the burst there is a strong negative OLR anomaly in the Indian Ocean, just south of the Bay of Bengal (80°E in Fig. 16, top). A positive OLR anomaly covers

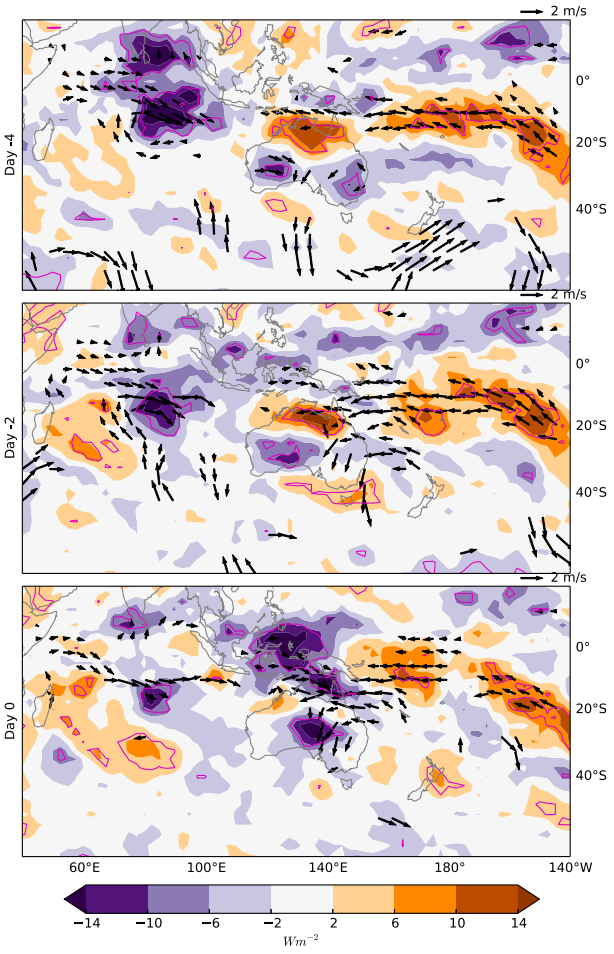

FIG. 16. As in Fig. 14, but for non-SF events (i.e., NF, EF, and WF).

the north of Australia, with low-level easterly trade winds prevailing from the Coral Sea to the northwest of Australia. Negative OLR anomalies cover the southern half of the Australian continent, while the wind vector anomalies show an anticyclonic anomaly over the Tasman Sea and a cyclonic anomaly to the south of Western Australia (120°E). A positive OLR anomaly spreads from the western Pacific Ocean (10°S, 180°) to the South Pacific (40°S, 140°W), suggesting a weakened South Pacific convergence zone (SPCZ).

Two days prior to the burst, the negative OLR anomaly over the Indian Ocean has spread into the Maritime Continent, while a line of negative OLR anomaly has strengthened along the equator to the northeast of Australia (Fig. 16, middle). This indicates a strengthening of the intertropical convergence zone (ITCZ). The positive OLR anomaly in the SPCZ region has also increased, and easterly wind anomalies dominate from the SPCZ right across the tropical north of Australia. The positive OLR anomaly in the Australian monsoon region has decreased in area, with a negative OLR anomaly strengthening over the southwestern Australian continent.

On the day of the burst, there is a negative OLR anomaly over much of the Maritime Continent, extending southward into the tropical north of Australia (Fig. 16, bottom). A negative OLR anomaly occurs over the Australian continent, consistent with a midlatitude trough, while a positive OLR anomaly remains in the SPCZ region. Northwesterly wind anomalies dominate the Australian monsoon region, with an anomalous cross-equatorial flow over the Maritime Continent.

The composite of all non-SF bursts shows a strong eastward moving negative OLR anomaly in the tropics, arriving in the Maritime Continent on the day of the burst. This pattern suggests that the MJO or other equatorial waves might play an important role in the initiation of non-SF bursts.

c. *The role of the MJO in Australian monsoon bursts*

Bursts categorized as not predominantly southerly influenced (non-SF bursts) may be more strongly modulated by tropical waves such as the MJO than the SF bursts. We investigate the influence of MJO phase on moisture flux convergence anomaly in Fig. 17. For the SF bursts, having an active MJO near the north of Australia (phases 3–6) did not have a significant influence on moisture flux convergence anomaly (at the 95% level). However, for the non-SF bursts there were more bursts diagnosed in phases 3–6, and these events had larger moisture flux convergence anomalies compared to the non-SF bursts in other phases of the MJO (significant at the 95% level).

5. Discussion and conclusions

The aim of this paper is to better understand the dynamics of Australian monsoon bursts, and the mechanisms that control the transition from break conditions to active convection. To do so we utilize the relationship between circulation tendency in a bounded region and the convergence of absolute vorticity flux into that region.

The net circulation in the monsoon region increases cyclonically in a shallow layer below 850 hPa prior to the composite monsoon burst (Fig. 2). The main mechanism changing the circulation prior to bursts is the convergence of planetary vorticity flux. An increase in low-level moisture flux convergence anomaly accompanies the cyclonic increase in circulation at the time the burst is initiated (Fig. 4).

Initially the largest contribution to absolute vorticity flux convergence and moisture flux convergence is through

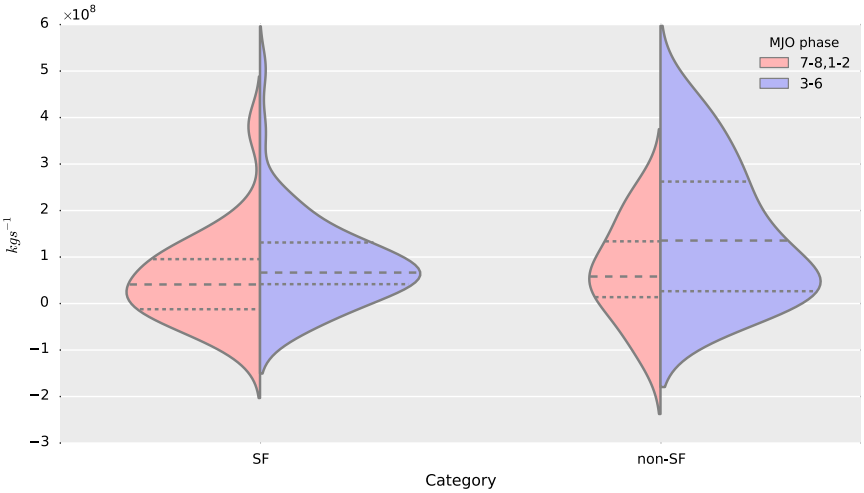

FIG. 17. Violin plots of column-integrated (from 1000 to 1 hPa) moisture flux convergence anomaly (10^8 kg s^{-1}) for (left) SF- and (right) non-SF-influenced bursts. Bursts in MJO phases 3–6 are plotted in blue, and all other phases in red. Only burst cases with amplitude of the Wheeler and Hendon (2004) MJO index greater than 1 were considered. The width of each violin represents the number of events in each category. The horizontal dashed lines correspond with the 25th, 50th, and 75th percentiles. The differences in the red and blue distributions (45 and 54 events, respectively) for the SF bursts were not significant above the 95% level. The differences in the red and blue distributions (16 and 36 events, respectively) for the non-SF bursts were significant above the 95% level.

the eastern boundary from the Coral Sea; however, these fluxes decrease as the burst commences, while the vorticity fluxes through the southern, northern, and western boundaries increase (Fig. 5). The Australian monsoon has traditionally been associated with a seasonal transition to "wet westerlies" over the north of Australia—the result of the eastward turning of a cross-equatorial flow pattern (Drosdowsky 1996). However, rainfall also occurs in association with easterly winds during the wet season. Drosdowsky (1996) attributed the easterly associated rainfall to the poleward side of either the monsoon trough or tropical cyclones. Pope et al. (2009) described a moist easterly regime over Darwin as the dominant state of the wet season, and they associated the easterly winds with monsoon break conditions. The results of our study show that the break conditions prior to the day of the burst are indeed dominated by easterly vorticity and moisture flux. Nevertheless, it is the changes in vorticity and moisture flux at the other boundaries, in particular the southern boundary, that determine the timing of the burst. We do not find that our burst categories are specifically related to any of the Darwin wet regimes; however, the occurrence of the deep westerly regime during bursts is greatest between December and February (not shown).

The lag composite of bursts shows that convective instability (represented by the modified K index) increases prior to the burst initiation, and that the change in convective instability is driven from the south of the monsoon region. The anomalies in the K index are found to be organized in the warm conveyor belt region of an approaching front and cyclone.

Prior to the burst there is an anomalous export of absolute vorticity out of the region, which quickly changes sign with the approach of the burst (Fig. 3). The change in circulation for the majority of individual monsoon bursts is most strongly correlated with the absolute vorticity flux through the southern boundary (Fig. 9). It is shown that around two-thirds of all bursts that are most strongly influenced by fluxes through the southern boundary (labeled as SF bursts in Fig. 10) occur throughout the wet season and outnumber all other burst categories in every month. The occurrence of SF bursts shows a strong seasonality, with a peak in November prior to the published climatological onset of the monsoon season in late December (e.g., Drosdowsky 1996). The dominance of SF bursts throughout the wet season is consistent with the results of Berry and Reeder (2016), who show that the synoptic pattern responsible for initiating bursts does not vary much throughout the wet season.

The synoptic pattern associated with SF bursts is a midlatitude Rossby wave train (Fig. 12). Several studies have highlighted such an extratropical–tropical interaction, although these have typically focused on onset of the Australian monsoon season rather than individual bursts. Davidson et al. (1983) showed that the Australian

monsoon onset seemed to require an alternating pattern of synoptic scale high and low pressure systems over the Australian continent. Davidson et al. (2007) showed that midlatitude Rossby wave refraction by the subtropical jet can influence monsoon onset, and this was supported with evidence from an idealized model. Another mechanism of extratropical influence is the advection of potential vorticity (PV) anomalies into the Australian monsoon region. Berry et al. (2012) found that heavy rainfall in the tropical north of Australia often occurred to the east of upper-level cyclonic PV anomalies, formed from the filamentation of PV anomalies of midlatitude origin that are advected along the east coast of the continent. In a study considering 14 cases of Australian monsoon onset, Hung and Yanai (2004) noted that all but one case involved the intrusion of midlatitude troughs into the monsoon region. The onset of rainfall occurred on the forward flank of these midlatitude troughs. It is interesting to note that 11 of their 14 onset dates coincide with a diagnosed monsoon burst, and the remaining onset dates are associated with rainfall events that very narrowly missed being diagnosed as bursts (not shown). Their onset dates were typically the first large (i.e., above 7 mm day^{-1}) or sustained (i.e., for several days) diagnosed burst of the season.

The intraseasonal variability of the Australian monsoon has been linked to the MJO (Hendon and Liebmann 1990b). Berry and Reeder (2016) showed that the initiation of individual rainfall bursts only has a weak relationship to the MJO, although they suggested that the MJO may influence the amount of rainfall produced. The calculation of a vorticity and moisture budget in this study provides an alternative approach to disentangling the factors (such as the MJO) that may influence the initiation of bursts. Bursts with a southerly influence (approximately two-thirds of all events) are found to only have a weak relationship with the MJO phase. However the non-SF bursts are found to have a stronger relationship with MJO phase, with more bursts occurring during MJO phases 3–6, when the MJO is in the vicinity of Australia (Fig. 17).

The simulation of the Australian monsoon in coupled climate models is highly variable, and future projections are largely uncertain (Moise et al. 2012). A consideration of the midlatitude influence highlighted in this study could improve our understanding of the Australian monsoon in weather and climate models.

Acknowledgments. This research is supported by the Australian Research Council Centre of Excellence for Climate Systems Science (CE1101028). AWAP data were provided by the Australian Bureau of Meteorology. ERA-Interim data were provided by the European Centre for Medium-Range Weather Forecasts.

REFERENCES

Berry, G. J., and M. J. Reeder, 2016: The dynamics of Australian monsoon bursts. *J. Atmos. Sci.*, **73**, 55–59, doi:10.1175/JAS-D-15-0071.1.

——, ——, and C. Jakob, 2011: A global climatology of atmospheric fronts. *Geophys. Res. Lett.*, **38**, L04809, doi:10.1029/2010GL046451.

——, ——, and ——, 2012: Coherent synoptic disturbances in the Australian monsoon. *J. Climate*, **25**, 8409–8421, doi:10.1175/JCLI-D-12-00143.1.

Charba, J. P., 1977: Operational system for predicting thunderstorms two to six hours in advance. NOAA Tech. Memo. NWS TDL-64, 24 pp.

Davidson, N. E., J. L. McBride, and B. J. McAvaney, 1983: The onset of the Australian monsoon during winter MONEX: Synoptic aspects. *Mon. Wea. Rev.*, **111**, 496–516, doi:10.1175/1520-0493(1983)111<0496:TOOTAM>2.0.CO;2.

——, K. J. Tory, M. J. Reeder, and W. L. Drosdowsky, 2007: Extratropical–tropical interaction during onset of the Australian monsoon: Reanalysis diagnostics and idealized dry simulations. *J. Atmos. Sci.*, **64**, 3475–3498, doi:10.1175/JAS4034.1.

Dee, D. P., and Coauthors, 2011: The ERA-Interim reanalysis: Configuration and performance of the data assimilation system. *Quart. J. Roy. Meteor. Soc.*, **137**, 553–597, doi:10.1002/qj.828.

Drosdowsky, W., 1996: Variability of the Australian summer monsoon at Darwin: 1957–1992. *J. Climate*, **9**, 85–96, doi:10.1175/1520-0442(1996)009<0085:VOTASM>2.0.CO;2.

Gill, J., 1999: The insignificance of null hypothesis significance testing. *Polit. Res. Quart.*, **52**, 647–674, doi:10.1177/106591299905200309.

Haynes, P. H., and M. E. McIntyre, 1987: On the evolution of vorticity and potential vorticity in the presence of diabatic heating and frictional or other forces. *J. Atmos. Sci.*, **44**, 828–841, doi:10.1175/1520-0469(1987)044<0828:OTEOVA>2.0.CO;2.

Hendon, H. H., and B. Liebmann, 1990a: A composite study of onset of the Australian summer monsoon. *J. Atmos. Sci.*, **47**, 2227–2240, doi:10.1175/1520-0469(1990)047<2227:ACSOOO>2.0.CO;2.

——, and ——, 1990b: The intraseasonal (30–50 day) oscillation of the Australian summer monsoon. *J. Atmos. Sci.*, **47**, 2909–2924, doi:10.1175/1520-0469(1990)047<2909:TIDOOT>2.0.CO;2.

Hung, C.-W., and M. Yanai, 2004: Factors contributing to the onset of the Australian summer monsoon. *Quart. J. Roy. Meteor. Soc.*, **130**, 739–758, doi:10.1256/qj.02.191.

Johnson, D. H., 1999: The insignificance of statistical significance testing. *J. Wildl. Manage.*, **63**, 763–772, doi:10.2307/3802789.

Jones, D. A., W. Wang, and R. Fawcett, 2009: High-quality spatial climate data-sets for Australia. *Aust. Meteor. Oceanogr. J.*, **58**, 233–248, doi:10.22499/2.5804.003.

Kilroy, G., R. K. Smith, M. T. Montgomery, B. Lynch, and C. Earl-Spurr, 2016: A case-study of a monsoon low that formed over the sea and intensified over land as seen in ECMWF analyses. *Quart. J. Roy. Meteor. Soc.*, **142**, 2244–2255, doi:10.1002/qj.2814.

——, ——, and ——, 2017: Tropical low formation and intensification over land as seen in ECMWF analyses. *Quart. J. Roy. Meteor. Soc.*, **143**, 772–784, doi:10.1002/qj.2963.

Liebmann, B., 1996: Description of a complete (interpolated) outgoing longwave radiation dataset. *Bull. Amer. Meteor. Soc.*, **77**, 1275–1277.

Moise, A. F., R. A. Colman, and J. R. Brown, 2012: Behind uncertainties in projections of Australian tropical climate: Analysis of 19 CMIP3 models. *J. Geophys. Res.*, **117**, D10103, doi:10.1029/2011JD017365.

Nicholls, N., 2001: Commentary and analysis: The insignificance of significance testing. *Bull. Amer. Meteor. Soc.*, **82**, 981–986, doi:10.1175/1520-0477(2001)082<0981:CAATIO>2.3.CO;2.

——, J. L. McBride, and R. J. Ormerod, 1982: On predicting the onset of the Australian wet season at Darwin. *Mon. Wea. Rev.*, **110**, 14–17, doi:10.1175/1520-0493(1982)110<0014:OPTOOT>2.0.CO;2.

Pope, M., C. Jakob, and M. J. Reeder, 2009: Regimes of the north Australian wet season. *J. Climate*, **22**, 6699–6715, doi:10.1175/2009JCLI3057.1.

Raymond, D. J., S. Gjorgjievska, S. Sessions, and Z. Fuchs, 2014: Tropical cyclogenesis and mid-level vorticity. *Aust. Meteor. Oceanogr. J.*, **64**, 11–25, doi:10.22499/2.6401.003.

Smith, R. K., M. T. Montgomery, G. Kilroy, S. Tang, and S. K. Müller, 2015: Tropical low formation during the Australian monsoon: The events of January 2013. *Aust. Meteor. Oceanogr. J.*, **65**, 318–341, doi:10.22499/2.6503.003.

Tan, J., C. Jakob, and T. P. Lane, 2013: On the identification of the large-scale properties of tropical convection using cloud regimes. *J. Climate*, **26**, 6618–6632, doi:10.1175/JCLI-D-12-00624.1.

Troup, A. J., 1961: Variations in upper tropospheric flow associated with the onset of the Australian summer monsoon. *Indian J. Meteor. Geophys.*, **12**, 217–230.

Wang, B., 2006: *The Asian Monsoon*. Springer, 787 pp.

Wheeler, M. C., and H. H. Hendon, 2004: An all-season real-time multivariate MJO index: Development of an index for monitoring and prediction. *Mon. Wea. Rev.*, **132**, 1917–1932, doi:10.1175/1520-0493(2004)132<1917:AARMMI>2.0.CO;2.

——, and J. L. McBride, 2005: Australian–Indonesian monsoon. *Intraseasonal Variability in the Atmosphere–Ocean Climate System*, W. Lau and D. Waliser, Eds., Springer, 125–173.